Dynamic Testing and Analysis of Heliostats to Evaluate Impacts of Wind on Optical Performance and Structural Fatigue

Clifford K. Ho, D. Todd Griffith, Jeremy Sment, Adam C. Moya, Joshua M. Christian, James K. Yuan, and Patrick S. Hunter

Sandia National Laboratories, Concentrating Solar Technologies Department, P.O. Box 5800, Albuquerque, NM 87185-1127, USA, (505) 844-2384, ckho@sandia.gov

Abstract

The impacts of dynamic wind loads on structural fatigue and optical performance of heliostats has been investigated in this paper. Modal analyses have been conducted both computationally and empirically to determine the modal shapes and frequencies of heliostats at the NSTTF. Results show that many of the modes that were measured empirically were matched by the simulations. However, modes that depended on the stiffness and damping of joints that were not rigorously modeled (e.g., elevation and azimuthal drives, roller joints) were not accurately simulated by the models. Wind loading spectra were identified that are likely to impact both fatigue and optical performance of heliostats. A low-frequency mean wind spectrum (say below 0.5 Hz) moves the structure in a quasi-static fashion (e.g. "sway of the heliostat"). A mid-frequency gust spectrum (~1 Hz) is defined by the fluctuating component of wind speed (i.e. the component of wind speed superimposed on the mean or average speed). Finally, vortex shedding corresponds to a broad range of frequencies caused by the shedding of vortices from the heliostat structure, which depends on the wind speed and a characteristic length. The study identified low-frequency (~1 – 2 Hz) rigid-body modes of vibration caused by backlash or slop in the gear drives, causing rigid-body rotation in the azimuthal and elevation directions. The optical performance of the NSTTF heliostat was evaluated for different modal shapes and gravity-induced deflections. Ray-tracing results showed that out-of-plane bending modes impacted the beam shape and centroid the most. Fatigue analyses were also performed using a commercial code to evaluate critical components and locations on the heliostat that were subject to fatigue from different modal shapes and the imposed stress cycles.

Keywords: Dynamic wind load, modal analysis, heliostat vibrations, fatigue analysis, ray tracing

1. Introduction

Heliostats constitute a majority (nearly 40%) of the direct costs of a concentrating solar power tower plant [1]. As a result, a significant amount of effort is being focused on designing and developing cheaper heliostats. The optical and structural performance of these new and existing heliostats under dynamic wind loads must be characterized and understood in order to meet both cost and performance objectives. Previous studies have focused on static wind loads using scaled models in wind-tunnel tests [2-5]. A few studies have evaluated dynamic effects (e.g., vortex shedding, vibrations) on heliostats or inclined flat plates, but nearly all of the published results have relied on small-scale models [4, 6-9]. This paper presents an overview of a U.S. DOE-sponsored program at Sandia National Laboratories' National Solar Thermal Test Facility (NSTTF) that includes dynamic testing and analysis of full-scale heliostats. The objectives of these tests and analyses are to characterize and understand the impacts of dynamic wind loads on heliostat optical performance and structural fatigue. A primary effort in 2012 has been to instrument multiple heliostats at the NSTTF to evaluate the impact of dynamic wind loads on heliostats at different locations within the field.

Keywords: modal analysis, heliostat, vibration, CFD, fatigue analysis, wind load

2. Approach

Individual heliostats ranging in size from 37 – 75 m^2 have been instrumented with accelerometers and strain

gauges to determine modal frequencies and shapes (Figure 1). Griffith et al. [10] provided details of the accelerometer installation, testing, and modal analysis of a single heliostat at the NSTTF. Dynamic response of the heliostats excited by both instrumented-impact-hammer and natural-wind inputs was recorded with a portable data acquisition system connected locally to the heliostat. Goals of these initial tests were to develop a better understanding of the fundamental heliostat dynamics through both test and finite element analysis, study the experimental response characteristics of the heliostat under wind loading, and evaluate suitable sensors for long-term monitoring. Recent work has developed a centralized data acquisition system for remote monitoring of multiple heliostats at the NSTTF. 3-D ultrasonic anemometers have also recently been installed on and near heliostats to (1) characterize the wind events that impact the heliostat vibrations and (2) determine which modes are most excited and impacted by wind. Finite element models of the heliostats have been developed to compare simulated modal shapes and frequencies with the test results [10, 11] and to predict optical and structural performance.

Figure 1. Left: Heliostat field at the NSTTF, Albuquerque, NM. Middle: Close-up of 37 m^2 heliostat. Right: Installing accelerometers and strain gauges on heliostat.

2.1. Modal, Optical, and Fatigue Analysis

2.1.1 Modal Test and Analysis

A now standard approach to evaluate the credibility of structural models used to predict system dynamic response is to perform a modal test. Modal tests provide a measurement of a structure's vibration properties called the modal parameters. These modal parameters include natural frequencies, damping, and mode shapes associated with individual modes of vibration. The modal parameters depend on the mass, damping, and stiffness properties of the structure, and are inherent properties of the structure that are independent of the loading conditions on the structure. These modal parameters can be readily computed using a finite element model and compared with the experimental measurements from the modal test. The reconciliation of the test observations and analysis predictions of the modal parameters provides a means to evaluate regions of the model geometry that may require refinement of the model parameters. The result of this process is a more accurate model that is useful for predicting response to dynamic loads (e.g., wind loading). The modal analyses were conducted using Solidworks Simulation and ANSYS Mechanical.

Modal tests are typically performed by recording dynamic response measurements that result from a known, quantified force input. A typical method is to use an instrumented impact hammer, which includes a force transducer to measure the input force excitation. The resulting dynamic response of the structure is recorded using accelerometers and sometimes strain gauges. This input/output methodology that leads to experimentally determining the modal parameters is the traditional approach in a modal test. However, sometimes it may be advantageous to record dynamic response that results from structural loads during normal operating conditions. Wind loading is a natural excitation that causes a dynamic response. Therefore, in these tests, operational response data due to wind loading was also recorded along with wind speed and direction and used to provide a second means for measuring the modal parameters. In addition, the operational wind-excited data is measured for actual operating conditions and provides a means to evaluate sensor characteristics and size of motions for a range of wind speeds, along with insight into which modes of vibration are most strongly excited by the wind.

2.1.2 Optical Analysis

The modal analyses provide deformed mode shapes which are used as inputs in an optical ray-tracing analysis that includes a sun power source, heliostat, and power tower target. This analysis evaluates impacts of modal deformations on beam shape and accuracy. Although the magnitudes of the displacements in the modal analysis are arbitrary, the modal displacements were scaled in the optical analysis to yield reasonable maximum displacements on the order of a centimeter. The deformed modal shapes were imported into the ray-tracing code APEX, which works as an add-on to the Solidworks CAD package. A heliostat (11W14) from the NSTTF was used in the analysis with elevation and azimuth angles defined by projecting a beam to the tower on Day 194 (July 13) at solar noon. The ray-tracing analysis implemented the following: (1) five million rays, (2) perfectly reflecting heliostat mirrors, and (3) perfectly absorbing target.

2.1.3 Fatigue Analysis

Structural fatigue analysis of the NSTTF heliostat was performed using ANSYS nCode DesignLife fatigue analysis software. The code utilizes finite element analysis results as inputs to obtain the stress on all locations of the structure under multiple simulated loading conditions, taking into account pre-stress and directional effects. The fatigue damage accumulated from the structure moving from one state of stress to another, as the structure moves between defined loading conditions, can then be calculated and used to produce an expected lifetime in terms of cycles to failure for each component of the structure. The finite element analysis used to obtain each state of stress for the fatigue calculation may be obtained from modal analyses, static loading simulations, or dynamic, coupled fluid-structural simulations. These simulations may be calibrated against experimentally collected data, such as measured wind speeds or observed strains at particular locations on the structure, such that the states of stress used as inputs to the fatigue calculation may be correlated to an observed time history of loading events. In this manner, the fatigue damage caused by field events may be predicted, and an overall structure lifetime can be evaluated based on the field events (i.e. wind storms, gusts) expected for a given time period. In this study, the stress distribution resulting from several bending modes (assuming a maximum deflection on the order of a centimeter) was used to determine the fatigue life of various heliostat components for purposes of illustration.

2.2. Anemometry and Wind Analysis

The anemometry strategy employs 10 three-dimensional ultrasonic anemometers (Vaisala WMT700) capable of measuring wind speed and direction in both azimuth and elevation. The sampling rate is set at 32 Hz. The anemometers are organized into a “field group,” a “portable group,” a “heliostat-mounted group,” and an “easterly wind group” (Figure 2).

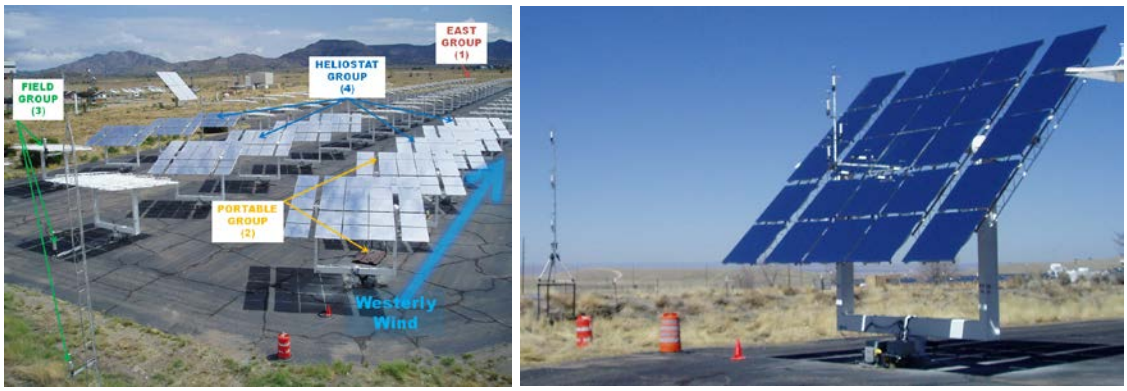

Figure 2. Left: Anemometer groups. Right: Photo of heliostat-mounted anemometers.

Three anemometers constitute the “field group” which is primarily used to characterize meteorological boundary wind conditions approaching the heliostat field from the west/southwest, which are the predominant wind directions in the spring and summer. The 10 meter field anemometer (F1) defines the reference meteorological wind speed (U_{ref}), azimuthal direction, and elevation. The second field anemometer (F2) defines the same information at the same height as the upper portable tower anemometer and the

heliostat-mounted anemometers (~6 m) for quick comparison of wind velocities across the heliostat field. The third field anemometer (F3) gives velocity information at the height of the heliostat torque tubes (~4 m).

In addition to the boundary wind velocity parameters, the data from the field group are used to define the reference wind speeds and the turbulence intensity. If a reference velocity (U_{ref}) of an atmospheric boundary layer wind is known at a reference height (h_{ref}), a power law is used to estimate the approaching wind speed (U_z) at any height (h_z) where $U_z = U_{ref}\left(\frac{h_z}{h_{ref}}\right)^{\alpha}$. α is defined as the slope of a curve fit through the data points of the log of anemometer heights vs. the log of the ratio of velocities $\frac{U_z}{U_{ref}}$. The boundary turbulence intensity of each velocity component is defined by the standard deviation of the respective component divided by the average of that same component.

Two anemometers constitute the "Portable Tower Group". The first anemometer is at the same height as the field anemometer (F2) and the heliostat mounted anemometers. The primary intention for this tower is to allow measurements of wind velocity at various rows and columns throughout the field. The portable tower can be located along various downstream rows giving an indication of velocities, wind dynamic pressure, and turbulence intensities. The "Heliostat Group" is comprised of one or more anemometers mounted on pipes affixed to the vertical yolk of the heliostat. The primary function of this group is to provide an input/reference for model validation. In the case of a west wind, heliostat-mounted anemometers are located in the third and fifth rows from the approaching wind. The heliostats selected for instrumentation were intended to evaluate wind impacts in the first 5 rows when westerly or southwesterly winds occurred. In the event of easterly winds, a single anemometer was placed on the eastern edge of the field. This anemometer can also be used for west-wind "back-row" wind studies.

2.3. Data Acquisition

A central data acquisition system was developed to monitor and analyze the structural dynamic behavior of the instrumented heliostats. Developed in the LabView programming environment (Figure 3), this system remotely acquires acceleration, strain, and wind data from a heliostat which is then streamed to a control tower via a fiber-optic communication line. The goal of this system is to fully characterize the natural frequencies and mode shapes exhibited by the heliostat when excited by hammer or wind input. One "well-instrumented" heliostat has been equipped with 24 tri-axial accelerometers and 4 strain gauges (Figure 3).

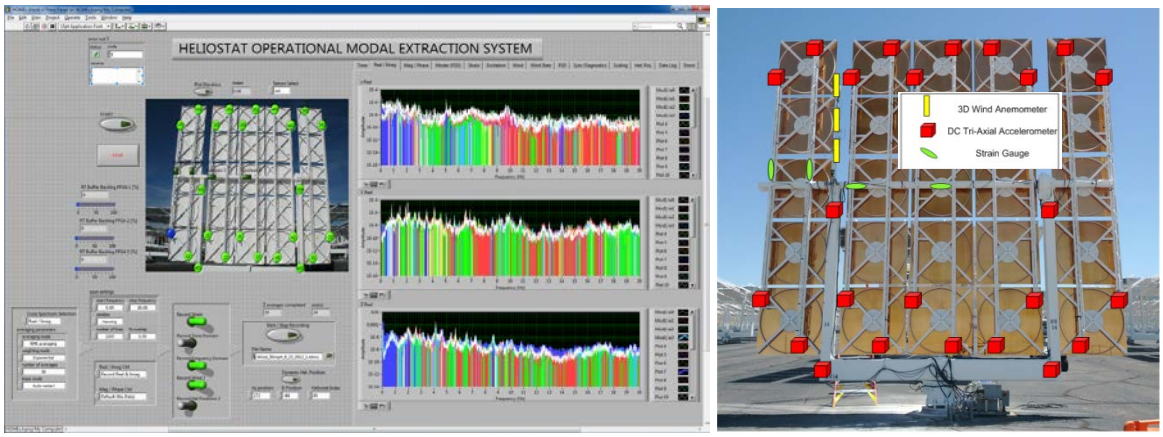

Figure 3. Left: Data acquisition system and interface for dynamic heliostat monitoring. Right: sensor placement for well-instrumented heliostat (11W14).

Another data acquisition system was created to monitor a number of heliostats throughout the field for wind and vibration excitation in real time. This field monitoring system consists of 11 nominally instrumented heliostats strategically placed in a triangular grid shown in Figure 4 with the goal of capturing winds characteristics and the heliostat modes that are excited. This system streams and logs acceleration, strain, and wind data from multiple locations simultaneously.

Data logging at 813 Hz can be triggered by wind events, hammer events, by time and date, or manually. Data logged includes accelerometer, strain, wind velocity, temperature and heliostat position. The well-instrumented heliostat utilizes a fiber optic data link while the nominally instrumented heliostats use the Telkonet system which bundles data information onto a single phase of the three phase power line for transmission to the control tower.

Processing allows real time presentation of wind velocity and strain across the instrumented portion of the field, as well as the meteorological site profile information such as turbulence intensity, power law coefficient, mean, standard deviation, etc. The user interface is adaptable to include more or less information within the display. Correlation matrices and t-test results between anemometers, strain, and rows of heliostats are displayed in a statistics tab. Position data is used to calculate the dynamically changing area used in the calculation of wind load coefficients and generalized blockage area.

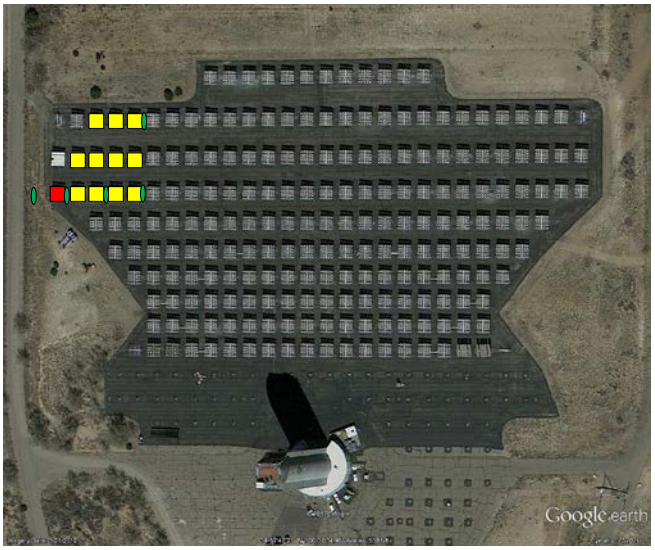

Figure 4: Nominally Instrumented Heliostats Respective Grid Locations

3. Results and Discussion

3.1. Modal Analysis – Hammer Excitation Results

Modal tests of the NSTTF heliostat using hammer excitation provided measurement of a number of modes of vibration [10, 11]. The dynamic behaviors identified included bending of the yoke (i.e the support structure), bending of the torque tube, in-plane and out-of-plane bending of the mirror/truss assemblies. Figure 5 shows an example of the simulated and empirical mode shapes for one of the 37 m^2 heliostats at the NSTTF excited by hammer impulse. The images shown in Figure 5 are for mode 4 of the heliostat, which is represented by in-plane bending of the torque tube at ~3.5 – 3.6 Hz. Results show that both the simulated and empirical mode shapes and frequencies are similar. To a large extent, the pre-test finite element predictions agreed well with the natural frequencies of the measured modes of vibration. However, modes with dependence on the stiffness properties of joints (elevation roller joint) and drive mechanisms (azimuth and elevation) were not as accurately predicted because they were modeled as rigid interfaces in the pre-test model. As a result of this modeling choice, out-of-plane bending modes associated with the yoke support structure were not accurately predicted. In addition, these initial modal tests demonstrated that modes of vibration associated with the azimuthal and elevation drive mechanisms (which were not modeled) existed at low-frequency and were excited by the wind. These so-called rigid-body modes of the drive mechanisms, in which the structure moves in a rigid fashion about the drive degree of freedom, are described in greater detail in this paper. Finite element models of modal shapes are being combined with optical ray-tracing models to quantify the

impact of wind excitation on optical performance. Data from the dynamic testing and analyses are also being integrated in structural analyses to evaluate wind impacts on structural fatigue and reliability.

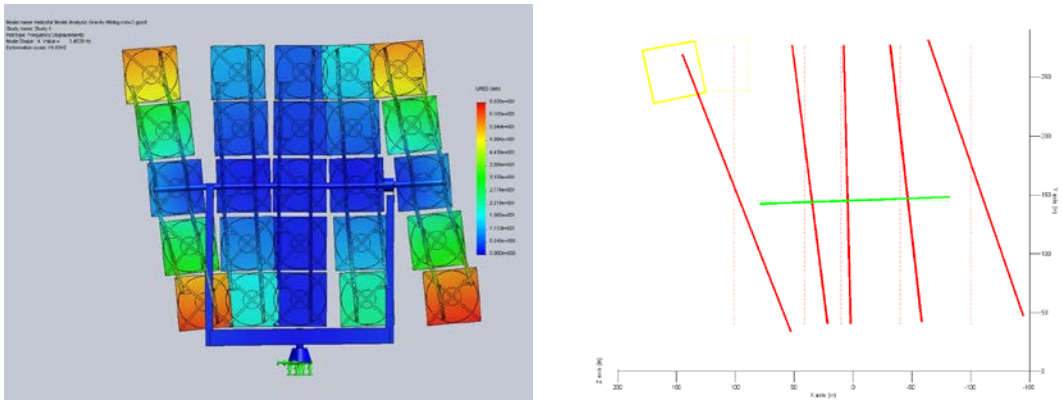

Figure 5. Right: Simulated modal shape for mode 4 (torque-tube bending at 3.45 Hz). Right: Experimental mode shape derived from accelerometer data at 3.57 Hz (red lines denote vertical trusses, the green line denotes the torque tube, and the yellow line denotes the upper-left facet).

3.2. Modal Analysis – Wind Excitation Results

Modes that are likely to be impacted by wind events are presented and discussed. As described in [11], modal parameters were identified from response-only measurements under dynamic wind loading. The experimentally identified frequencies were in very close agreement with those from the hammer-excited tests. However, the damping was significantly higher for the wind-excited tests. For the hammer tests, wind speeds were calm or very low; therefore, the damping estimates only include the inherent structural damping mechanism. For the wind-excited tests, the measured damping was higher and included both the structural damping as well as aerodynamic damping from the wind.

Table 2 shows the extracted damping values for a few of the modes of vibration. Damping is shown for two wind speed magnitudes: (1) zero or calm (hammer tests) and (2) high winds at 10-30 mph (wind excited). It was expected that the aerodynamic component of damping is proportional to wind speed, and these measurements confirm this intuition. The results show that damping increases in the range from 24 to 120% for this set of in-plane bending modes at higher wind speeds. Although not tabulated, analysis of damping for modes with out-of-plane motion shows even larger increases of 200% or more. The modes of vibration of this heliostat are very lightly damped (< 0.5%) even with the increased aerodynamic damping.

Table 1. Damping Values with Wind Speed Magnitude (0 degree configuration)

Mode No.	Mode Description	Pretest Predicted Frequency(Hz)	Damping (%) Calm	Damping (%) 10-30 mph
1	Yoke Bending (in-plane)	1.604	0.235	0.299
3	1st Torque Tube Bending	3.002	0.117	0.228
4	2nd Torque Tube Bending	3.453	0.183	0.402
7	In-plane Bending (2)	3.879	0.257	0.319

Strain measurements also indicated the suitability of dynamic strain gauges for this test application. These sensors performed extremely well with excellent low noise characteristics. Strain time histories were recorded which demonstrated a relation with the wind speed, and which demonstrated large response at the modal frequencies. The performance of these gauges for strain measurement due to dynamic loads is

superior to traditional strain sensors as the sensitivity is much higher permitting meaningful measurement of strain for even very low wind speeds. Although the sensitivity of these strain sensors is high, a well-known difficulty in using strain gauges is lack of certainty in measurement sensitivity with the glued mount. Determination of frequency and damping information is possible with very good accuracy; however, determination of mode shapes or estimation of strain or displacement amplitude has greater uncertainty.

3.2.1 Wind Loading Spectra

The initial studies [12] have led to consideration of three distinct wind loading phenomena, which each produce loads on the structure in different frequency ranges: (1) **Mean Spectrum**: At low-frequency (say below 0.5 Hz) the mean or average wind loading is significant and moves the structure in a quasi-static fashion (e.g. "sway of the heliostat"). This effect is evidenced by the power spectrum of the wind speed as it demonstrates the significant low-frequency content in the wind speed and roll-off in its magnitude at higher wind speeds; (2) **Gust Spectrum**: At mid-frequency (~1 Hz) the gust loading spectrum is important. Here the fluctuating component of wind speed (i.e. the component of wind speed superimposed on the mean or average speed) produces loads at higher frequencies and in the frequency range of structural modes of vibration of a typical heliostat; and (3) **Vortex Shedding**: In addition to the mean and gust spectrums, vortex shedding phenomena is important for heliostat structures. The frequency at which vortex shedding occurs may be essentially anywhere in the frequency spectrum associated with structural modes of vibration because it varies with wind speed and the apparent size of the structure. Vortex shedding is of particular concern when the frequency of vortices shed from the structure matches a structural resonance (i.e a mode of vibration).

With respect to fatigue, a primary concern in heliostat design is durability of the drive mechanisms. Therefore, characterization of the rigid body modes in the azimuth and elevation drives and how they are excited by the dynamic wind load is critical in design. Gust spectrum is a concern for drive mode excitation when the gust frequency coincides with the modal frequency. Vortex shedding is also a concern for drive mode excitation, when the shedding frequency coincides with a modal frequency. The objective is to design (or operate) the structure so as to avoid wind loads that cause high-amplitude or high-cycle counts in the drive components that result from either of these two dynamic load phenomena. With respect to optical accuracy, a designer is concerned with excessive motion of the mirrors in response to the wind loads. Here, all three wind loading effects described above are a concern for optical accuracy as each of these wind loading effects can cause motions (translations and rotations) of the mirrors.

Considering the above three wind loading characteristics and their potential impact on fatigue and optical design concerns, an instrumentation plan was developed so that each of these issues could be studied further through observation and experimental data analysis. Although the initial modal tests provided some very valuable information and provided us with an initial hypothesis about the effects of wind loading, we also desired to design the instrumentation to enable new discovery and measurement of phenomena that may not have occurred in the earlier limited duration observations. For example, the initial tests were only performed for three different orientations about the elevation degree of freedom; however, vortex shedding may occur over a wide range of wind speeds and for virtually any particular orientations of the heliostat with respect to the wind direction. The long-range monitoring tests will enable characterization of wind loading events for all operating configurations and for a wide range of wind velocity conditions.

In order to measure the low-frequency mean spectrum response, DC accelerometers were procured as they are capable of measuring acceleration response down to 0 Hz. Traditional piezoelectric accelerometers were also selected as they provide good measurement characteristics for gust spectrum loading and vortex shedding. However, the piezoelectric accelerometers are not capable of measuring response below 0.5 Hz. On the other hand, DC accelerometers have difficulty in measuring at higher frequencies. Therefore, use of both types of sensors offers a more robust approach to characterization of the fatigue and optical events that are of interest with their complimentary characteristics.

3.2.2 Rigid Body Motion in Drive Mechanisms

A key observation in these studies is the presence of low-frequency modes of vibration associated with the azimuth and elevation drives. We refer to these as rigid body modes because these modes involve motion only in the rotational degrees of freedom of the associated drive and do not involve any deformation in the structure. In the prior modal tests [10, 11], the azimuth rigid body mode was found to be the lowest frequency mode of the structure at a frequency of 1.28 Hz. The importance of these rigid body drive modes is that due to their low frequency behavior, they are at greater risk to be more strongly excited by the wind.

Analytically, the frequency of a drive mode can be modeled very accurately with a simple model of the form:

$$f = \frac{1}{2\pi}\sqrt{\frac{k_\theta}{I_\theta}}$$

Where f is frequency in Hz, k_θ is the stiffness associated with drive rotation, and I_θ is the mass moment of inertia associated with the part of the structure that is moving. For the azimuth rigid body mode, which is the focus of this particular investigation, the rotational stiffness in this equation is simply the stiffness associated with rotation in the azimuth mechanism and the mass moment of inertia is associated with the entire structure of the heliostat above the azimuth drive. Of course, the mass moment of inertia is dependent upon the orientation of the elevation drive, and the frequency of the azimuth drive will be dependent upon mirror orientation.

To illustrate these points and demonstrate additional characteristics of the azimuth drive modes that have been observed experimentally, we now describe additional modal test results for the 37 m^2 NSTTF heliostat as well as a commercial heliostat with ~60 and ~80 m^2 mirror areas. For the commercial unit, only the mirror area is a variable as the drive mechanism, pedestal arrangement and height were unchanged.

Table 2 provides a list of azimuth drive mode frequencies identified from modal tests using hammer impact excitation. The data in the table is intended to demonstrate the dependence of the modal frequency on the mass moment of inertia of the mirror assembly. Both the mirror size and mirror orientation affect the mass moment of inertia magnitude. For the NSTTF heliostat, one can see that the modal frequency drops as the mass moment of inertia of the mirror assembly about the azimuth degree of freedom is increased toward the stowed or 90 degree orientation (while the drive rotation stiffness is unchanged). In our tests, we had the opportunity to evaluate the azimuth rigid body mode for a commercial heliostat unit having ~60 m^2 area and the ability to increase the area to ~80 m^2 with simple addition of mirror structure. Tests were again performed at 0, 45, and stowed (90 degree) orientations of the elevation drive. As can be seen in Table 2, the azimuth rigid body modal frequency drops with increasing mass moment of inertia. For the larger mirror area, the mass moment of inertia increases and with constant stiffness in the drive, the frequency is decreased.

Table 2. **Azimuth drive modal frequency variation with mirror orientation and mirror size**

Heliostat Designation	Heliostat Mirror Area (m^2)	0 degree orientation (vertical)	45 degree orientation	90 degree orientation (stowed)
NSTTF	37	1.28	1.09	1.04
Commercial Unit	~60	2.28	1.98	1.75
Commercial Unit	~80	1.55	~1.4	~1.3

The damping of the azimuth rigid body modes was very high compared with the other heliostat modes of

vibration. For the NSTTF heliostat, damping was found to be in the range of 5-15% of critical damping, although the estimates of damping were found to have greater uncertainty at the low end of this damping range. The other modes of the heliostat were less than 1% damped even for high wind speed cases with increased aerodynamic damping. For the commercial heliostat configurations, damping was found to be in the range of 7-10% of critical damping and was not found to be significantly affected by the change in mirror area size. The contact of the gear teeth in the drive mechanism dictates both the stiffness and damping of the drive.

This summary provides some important results pertaining to the dynamic response in the drive mechanism, and can provide important design information related to fatigue life estimation. Mirror area affects the frequency of the azimuth drive mode, and in addition this mode is strongly dependent on orientation of the mirror assembly.

3.2.3 Impacts of Vortex Shedding on Rigid Body Modes

One particular concern is vortex shedding and its coincidence with the azimuth rigid body modal frequency. Here we summarize a parameter study for a few heliostat configurations. The vortex shedding frequency, f (Hz), is given by the Strouhal number, St, wind velocity, V (m/s), and characteristic length, D (m):

$$f_{shedding} = \frac{St\,V}{D}$$

The Strouhal number is a non-dimensional number that depends on the shape of the body and the Reynolds number of the wind flow; however, a typical value for flat plates is 0.14 [13] for the range of Reynolds numbers experienced. The wind speed depends on the relative orientation of the wind direction and the heliostat's orientation. Likewise, the characteristic length also depends on this relative orientation. Assuming that the Strouhal number is a constant, the shedding frequency will then be proportional to the ratio of wind speed (V) to characteristic length (D). Choosing a value for the Strouhal number of 0.14 as indicated earlier, which is appropriate for this application based on prior works for flat plates, we compute the shedding frequency for some typical wind speed and characteristic length pairs in Table 3. The results show that for typical wind speeds in the range of 1 to 12 m/s (2 to 27 miles per hour), a smaller characteristic length results in shedding frequencies near that of the azimuth drive rigid body mode found to be between 1 – 2 Hz (see highlighted cells). The smaller value of D corresponds to a near-stowed heliostat position when the wind is "edge-on" to the mirror assembly. One observation here is that vortex shedding can occur at relatively small wind speeds when stowed or near stowed. Although this is only a conceptual exercise to demonstrate a potential method to evaluate vortex shedding associated with the azimuth drive, it could also be applied to various other orientations of the mirror assembly to evaluate possible vortex "lock-in" behavior for other structural modes of vibration.

Table 3. Vortex shedding frequency, $f_{shedding}$, for different wind velocities (V) and characteristic lengths (D). Highlighted cells denote frequencies corresponding to rigid-body modes of vibration.

***V* (m/s)**	***D* (m)**						
	0.25	**0.5**	**1**	**2**	**4**	**8**	**16**
1	0.56	0.28	0.14	0.07	0.04	0.02	0.01
2	1.12	0.56	0.28	0.14	0.07	0.04	0.02
4	2.24	1.12	0.56	0.28	0.14	0.07	0.04
6	3.36	1.68	0.84	0.42	0.21	0.11	0.05
8	4.48	2.24	1.12	0.56	0.28	0.14	0.07
10	5.60	2.80	1.40	0.70	0.35	0.18	0.09
12	6.72	3.36	1.68	0.84	0.42	0.21	0.11

3.3. Wind Analysis Results

Dynamic strain data and wind velocity is being used to correlate wind velocity, strain magnitude, and relative row position. Peterka's wind load reduction theory suggests that wind load coefficients are a function of "generalized blockage area" (the projected solid area blocked by upstream heliostats divided by the ground area occupied by the same heliostats) up to the fourth row; the coefficients then level off such that the fifth row and beyond have relatively constant values [14]. Peterka's cited research used a staggered heliostat array pattern where the odd rows align in odd numbered columns and the even row heliostats align in the even numbered columns. The NSTTF field has all rows aligning in all columns so the "leveling off" effect predicted in the fifth numbered row may be expected earlier at the NSTTF. The heliostats are instrumented with piezoelectric dynamic strain gauges. A significant and consistent decrease in relative strain magnitude or decreasing wind velocities as measured on the portable anemometer tower correlated with in-field row position can be associated with the existence of a wind load reduction phenomenon. Additionally, data from heliostat mounted anemometers will be analyzed for significant correlations.

A primary goal for this research is to inform and develop models that can be used to predict wind loading in a variety of field configurations, heliostat designs, and wind conditions. Preliminary computational fluid dynamics models have been developed to determine whether a decreasing wind velocity trend can be predicted using computational fluid dynamics. Preliminary model results are inconclusive (Figure 6), but additional refinement and more rigorous computational simulations are being pursued.

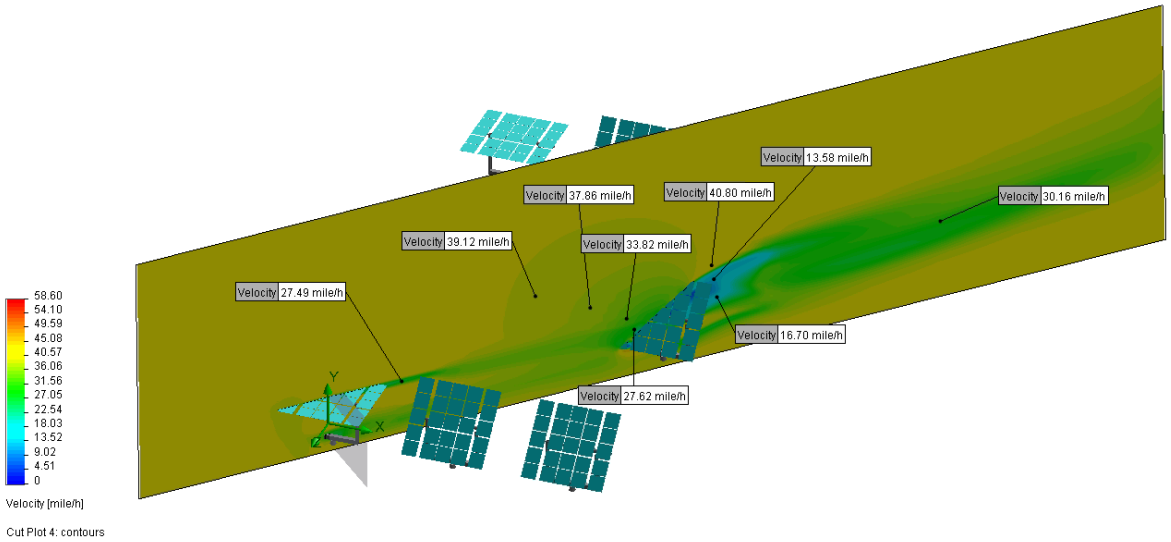

Figure 6. Example of simulated wind velocity distribution to predict the existence of decreased wind loading phenomenon.

3.4. Optical Analysis Results

Figure 7 depicts several possible deformed mode shapes and the resultant simulated beam image on a target approximately 200 m away (132 m to the west, 137 m to the south, and 29 m above the heliostat). The mirror surfaces are deformed due to gravity and the mode shapes, but additional slope errors which would account for manufacturing defects, cleanliness, etc. are not included. Mode 1 depicts the mirrors moving together as the support structure bends. The beam centroid for this mode does not translate a large amount, but the flux distribution has changed. Mode 2 depicts mirror out-of-plane motion such that the mirror surfaces do not lie in a similar plane. This mode gives the worst beam shape including a large change in centroid location and decrease in the flux distribution. Modes 3 and 12 depict mirror in-plane motion such that the mirror surfaces lie in a similar plane, but translate in that plane. The effects on beam shape are not as significant as out-of-plane motion, but some beam spreading still occurs. Table 4 summarizes the relative beam centroid displacements resulting from the various mode shapes.

Model Description	Deformed Image (Exaggerated Scale)	Beam Shape (Legend: 0-9000 W/m^2)
No Deformation	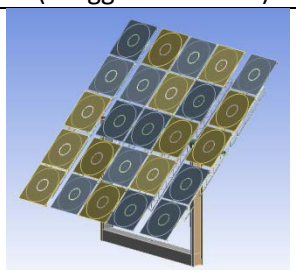	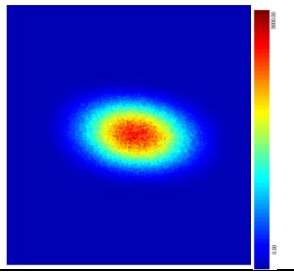
Mode Shape 1	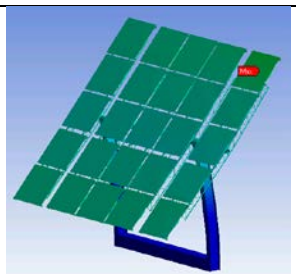	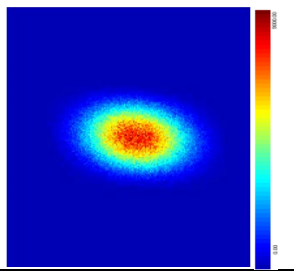
Mode Shape 2	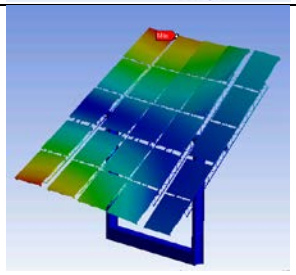	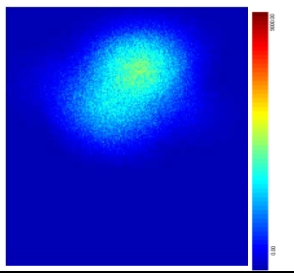
Mode Shape 3	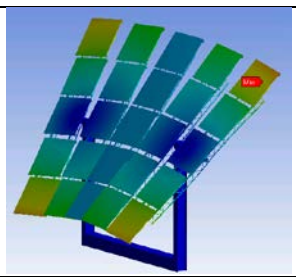	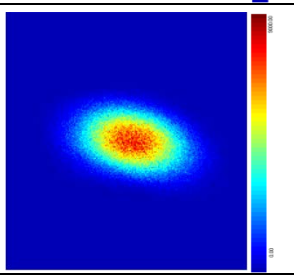
Mode Shape 12	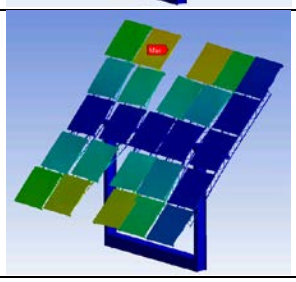	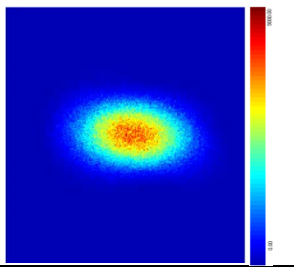

Figure 7. Heliostat deformed shapes and corresponding beam shapes, beam shapes are located on tower with the positive direction to the left and up

Table 4. Relative deviations of beam centroid location for different models. Negative values denote a translation to the right or down on tower (viewing tower target).

Model	Horizontal Deviation (m)	Vertical Deviation (m)
No Deformation	0.000	0.000
Gravity Deformation	0.102	-0.250
Mode 1	-0.042	-0.003
Mode 2	0.169	1.576
Mode 3	0.008	-0.019
Mode 12	-0.028	0.027

3.5. Fatigue Analysis Results

A preliminary fatigue analysis was performed on four selected mode shapes likely to be excited by wind. Deflections for each simulated mode shape were scaled to obtain the resulting stresses in the heliostat structure. The deflection magnitude was chosen to produce levels of stress above the endurance limit of the material, in order to highlight critical areas of the structure vulnerable to fatigue damage. With accurate characterization of deflections for each excited mode shape, a more rigorous evaluation of structure lifetime can be performed, in terms of a survivable number of cycles, with one cycle defined as the heliostat moving from the un-deformed shape to the excited mode shape, and then returning to the un-deformed shape. Table 5 shows each mode shape and the fatigue results for the structure, with potentially problematic areas highlighted.

Table 5. Structure locations with accumulated fatigue damage for selected mode shapes.

Mode shape	Fatigue Affected Areas		Reported Life (Number of Cycles to Failure)
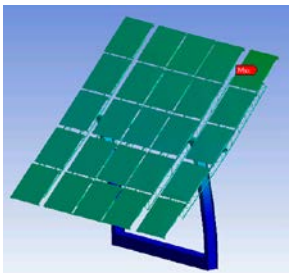 Mode 1	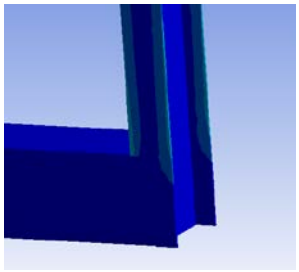 Yoke Beam Corner	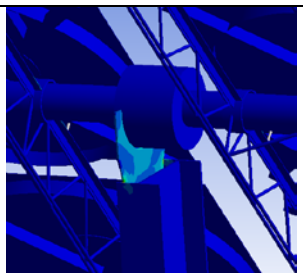 Yoke Beam to Drive Connection	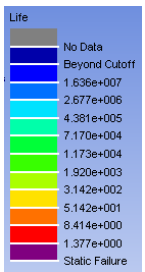
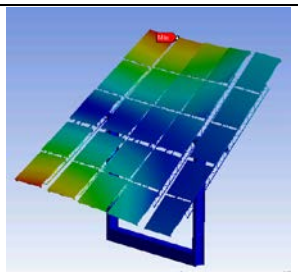 Mode 2	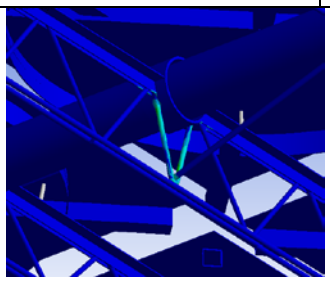 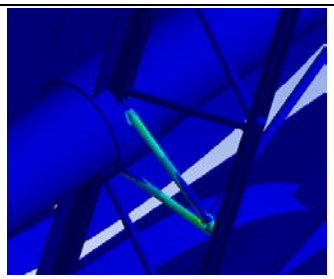 Truss Cross Members at Torque Tube		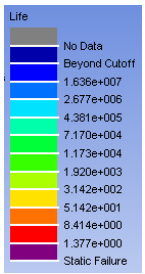

Mode shape	Fatigue Affected Areas		Reported Life (Number of Cycles to Failure)
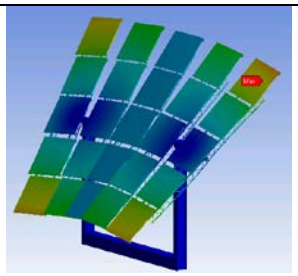 Mode 3	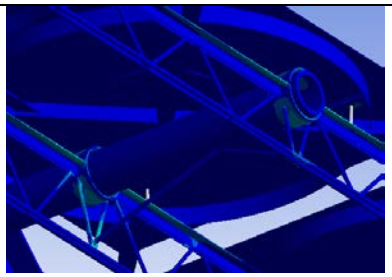 Torque Tube and Truss Interface, and Top Truss Chord		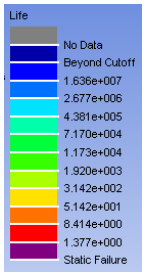
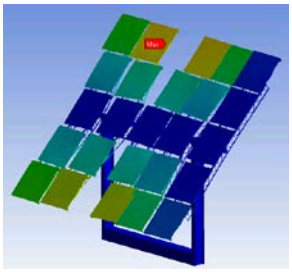 Mode 12	 Top Truss Chord	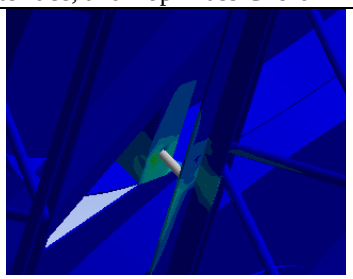 Mirror Bracket to Truss Connection	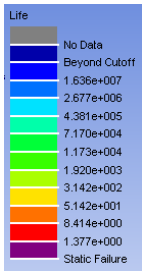

Results suggest that the joints of the structure, such as the interfaces between the elevation drive and yoke beam for mode 1, and the truss member to torque tube interfaces for modes 2, 3, and 12 experience greater stress and are more vulnerable to fatigue damage. Less apparent locations such as the connection between the truss chord and mirror bracket may also accumulate damage, as seen in mode 12. Without precise characterization of mode shape deflection magnitudes, reported cycle lifetimes are not yet physically significant. Nonetheless, the analysis is useful for identifying areas of the structure that may need reinforcement to increase fatigue life, and areas which may be optimized to reduce costs without impacts on structure life.

4. Summary

The impacts of dynamic wind loads on structural fatigue and optical performance of heliostats has been investigated in this paper. Accelerometer (both AC and DC to capture a wide range of vibration frequencies), dynamic strain gauges, and anemometers have been deployed on full-scale heliostats at the National Solar Thermal Test Facility (NSTTF) to monitor and evaluate the impacts of dynamic wind loads. Modal analyses have been conducted both computationally and empirically to determine the modal shapes and frequencies of heliostats at the NSTTF. Results show that many of the modes that were measured empirically were matched by the simulations. However, modes that depended on the stiffness and damping of joints that were not rigorously modeled (e.g., elevation and azimuthal drives, roller joints) were not accurately simulated by the models.

The study identified low-frequency (~1 – 2 Hz) rigid-body modes of vibration caused by backlash or slop in the gear drives. The frequency of these rigid-body modes increased with increased mass of the heliostat structure for a fixed stiffness. The damping of the rigid-body modes (~10 – 15% of critical damping) was found to be significantly higher than the damping associated with the heliostat structure, even with aerodynamic damping (less than 1% of critical damping).

Wind loading spectra were identified that are likely to impact both fatigue and optical performance of heliostats. A low-frequency **mean wind spectrum** (say below 0.5 Hz) moves the structure in a quasi-static fashion (e.g. “sway of the heliostat”). A mid-frequency **gust spectrum** (~1 Hz) is defined by the fluctuating component of wind speed (i.e. the component of wind speed superimposed on the mean or average speed).

Finally, **vortex shedding** corresponds to a broad range of frequencies caused by the shedding of vortices from the heliostat structure, which depends on the wind speed and a characteristic length.

The optical performance of the NSTTF heliostat was evaluated for different modal shapes and gravity-induced deflections. Results showed that out-of-plane bending modes impacted the beam shape and centroid the most. Fatigue analyses were also performed using a commercial code to evaluate critical components and locations on the heliostat that were subject to fatigue from different modal shapes and the imposed stress cycles.

Acknowledgments

Sandia National Laboratories is a multi-program laboratory managed and operated by Sandia Corporation, a wholly owned subsidiary of Lockheed Martin Corporation, for the U.S. Department of Energy's National Nuclear Security Administration under contract DE-AC04-94AL85000.

References

[1] Kolb, G.J., Ho, C.K., Mancini, T.R., Gary, J.A., 2011, Power Tower Technology Roadmap and Cost Reduction Plan, SAND2011-2419, Sandia National Laboratories, Albuquerque, NM.

[2] Peterka, J.A. and R.G. Derickson, 1992, Wind Load Design Methods for Ground-Based Heliostats and Parabolic Dish Collectors, SAND92-7009, Sandia National Laboratories, Albuquerque, NM.

[3] Pfahl, A., M. Buselmeier, and M. Zaschke, 2011, Wind loads on heliostats and photovoltaic trackers of various aspect ratios, *Solar Energy*, **85**(9), p. 2185-2201.

[4] Wu, Z.Y., B. Gong, Z.F. Wang, Z.N. Li, and C.C. Zang, 2010, An experimental and numerical study of the gap effect on wind load on heliostat, *Renewable Energy*, **35**(4), p. 797-806.

[5] Rebolo, R., J. Lata, and J. Vazquez, 2011, *Design of Heliostats Under Extreme and Fatigue Wind Loads*, in *in proceedings of SolarPACES 2011*, Granada, Spain, September 20-23, 2012.

[6] Chen, J.M. and Y.C. Fang, 1996, Strouhal numbers of inclined flat plates, *Journal of Wind Engineering and Industrial Aerodynamics*, **61**(2-3), p. 99-112.

[7] Gong, B., Z.N. Li, Z.F. Wang, and Y.G. Wang, 2012, Wind-induced dynamic response of Heliostat, *Renewable Energy*, **38**(1), p. 206-213.

[8] Wang, Y.G., Z.N. Li, B. Gong, and Q.S. Li, 2009, Wind Pressure and Wind-induced Vibration of Heliostat, *Advances in Concrete and Structures*, **400-402**, p. 935-940.

[9] Huss, S., Y.D. Traeger, Z. Shvets, M. Rojansky, S. Stoyanoff, and J. Garber, 2011, *Evaluating Effects of Wind Loads in Heliostat Design*, in *in proceedings of SolarPACES 2011*, Granada, Spain, September 20-23, 2012.

[10] Griffith, D.T., A.C. Moya, C.K. Ho, and P.S. Hunter, 2011, *Structural Dynamics Testing and Analysis for Design Evaluation and Monitoring of Heliostats*, in *Proceedings of ASME 2011 5th International Conference on Energy Sustainability & 9th Fuel Cell Science, Engineering and Technology Conference*, ESFuelCell2011-54222, Washington, DC, August 7-10, 2011.

[11] Griffith, D.T., C.K. Ho, P.S. Hunter, J. Sment, A.C. Moya, and A.R. Menicucci, 2012, *Modal Analysis of a Heliostat for Concentrating Solar Power*, in *in Proceedings of the 30th International Modal Analysis Conference (IMAC XXX)*, Jacksonville, FL, January 30 - February 2, 2012.

[12] Abanades, S., P. Charvin, and G. Flamant, 2007, Design and simulation of a solar chemical reactor for the thermal reduction of metal oxides: Case study of zinc oxide dissociation, *Chemical Engineering Science*, **62**(22), p. 6323-6333.

[13] Strickland, J.H., R.R. Matty, and G.H. Barton, 1980, Vortex Shedding from Square Plates Perpendicular to a Ground Plane, *Aiaa Journal*, **18**(6), p. 715-716.

[14] Peterka J.A., R.G.D., 1992, Wind Load Design Methods for Ground Based heliostats and Parabolic Dish Collectors, Colorado Stae University, Fort Collins, Colorado.